Chapter 10　Automatic film thickness measurement system for ink-jet type color filters

10.1 Background and objectives of the study

With the trend toward larger and cheaper flat panel displays, the color filter manufacturing method using the inkjet method (hereinafter referred to as "IJ method") is becoming more and more important. Since the IJ method uses a large number of IJ nozzles, the film thickness of each cell (hereinafter referred to as "cell" to distinguish it from the camera pixel) is more likely to fluctuate than in the conventional photo-lithography method. Therefore, the cell film thickness is an important control item. However, there is no fast, accurate and robust film thickness measurement technique.

In order to solve this problem, we have developed an automatic film thickness measurement system with high speed and high accuracy using single-shot interferometry. As shown in Fig. 10-1(a), the film thickness can be obtained from the measured surface profile by installing empty cells at the top and bottom of each measurement field of view, as shown in Fig. 10-1(b). Because the film contains pigments and is opaque, the backside reflection light can be ignored. Therefore, we adopted a method of measuring film thickness from the surface profile.

In this chapter, various elemental techniques for the system and test results are described.

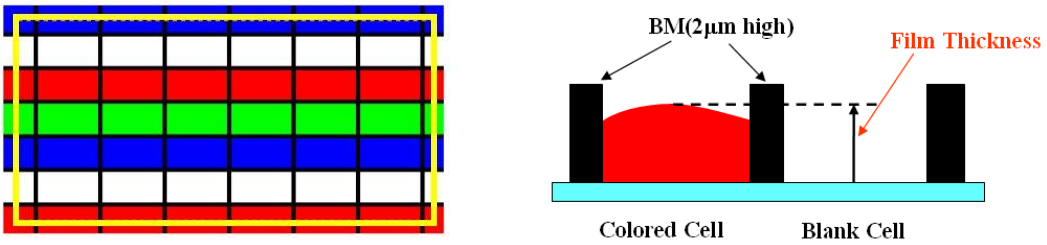

(a) Substrate pattern　　(b) Film thickness

Fig. 10-1 Color-filter substrate and its film thickness measurement

10.2 Selection of fringe direction

10.2.1 Background and objectives of the study

The surface of the cell is convex with a slightly raised center as shown in Fig. 10-1 (b), and this surface flatness is also an important measurement item. Since the shape of the cell is rectangular, the longitudinal surface profile is important.

On the other hand, perhaps because the single-shot interferometry with the carrier fringe introduction method has been studied since the 1990s, most of the reports introduce vertical fringes in the image and analyze the waveform of the horizontal video signal of a camera (Fig. 1-9). Up to this point in this paper, we also have been consistently introduced vertical fringes. However, from the point of view of current digital image processing technology, there is no restriction on the direction of the fringes, and it is necessary to discuss the fringe direction from another point of view.

In this section, we examine which fringe direction is better, vertical or horizontal, for obtaining the longitudinal profile of a cell based on the theoretical considerations and experiments.

10.2.2 In the case of step surface samples

(1) Theoretical considerations

In this paper, we discuss what kind of difference occurs between vertical and horizontal fringe directions when the groove direction (i.e., the step direction) is vertical, as has been the case in our previous experiments. When the fringe direction is vertical, the carriers are on the horizontal intensity signal, which is orthogonal to the vertical direction, as shown in Fig. 10-2(a). Since there is a sudden phase change in the stepped area, accurate phase detection is not possible in the vicinity by either the Fourier transform method or the LMF method, high frequency components are lost, and the measurement error becomes large.

On the other hand, when the fringe direction is horizontal, as shown in Fig. 10-2(b), the carrier is in the longitudinal direction and the signal is sinusoidal with a constant phase, so that accurate measurement is possible even in the vicinity of a step.

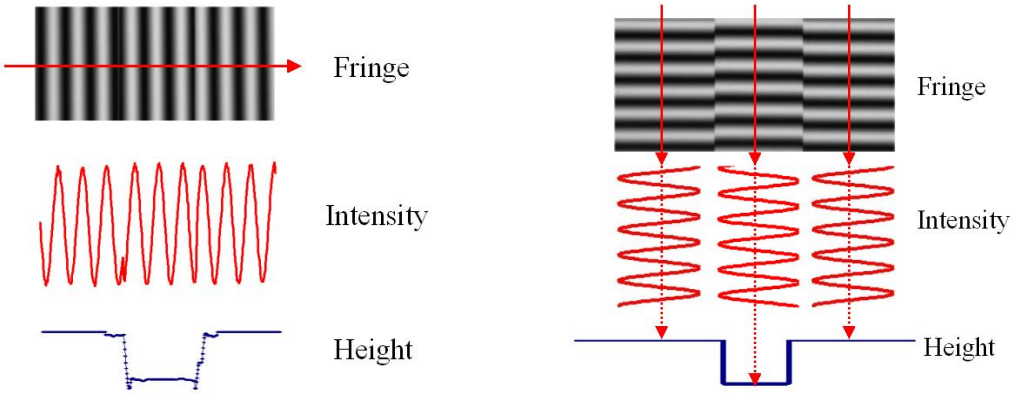

(a) Horizontal fringe (b) Vertical fringe

Fig. 10-2 Effect of fringe direction

(2) Actual experiments

The 50-nm standard step of the concave shape used in Chapter 6 was measured in different fringe directions. The images for vertical, horizontal and slanted fringes and the *x, y* profiles of the measurement results are shown in Figs. 10-3, 10-4 and 10-5. It can be seen that the horizontal stripes are best for horizontal (*x*-axis) profiles and the vertical fringes are best for vertical (*y*-axis) profiles.

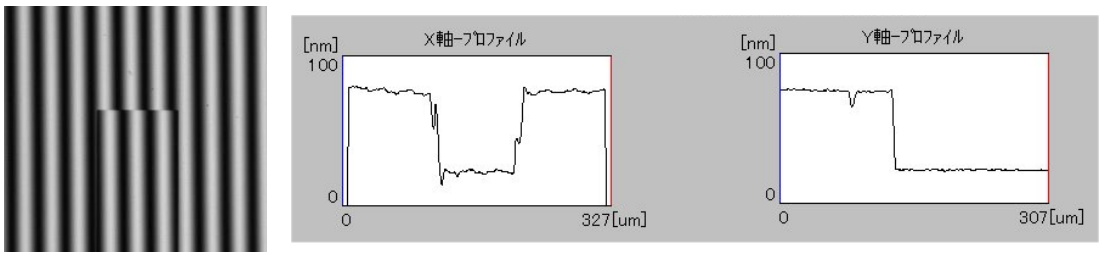

(a) Fringe image (b) Obtained surface profiles

Fig. 10-3 Vertical fringe image and its measurement results

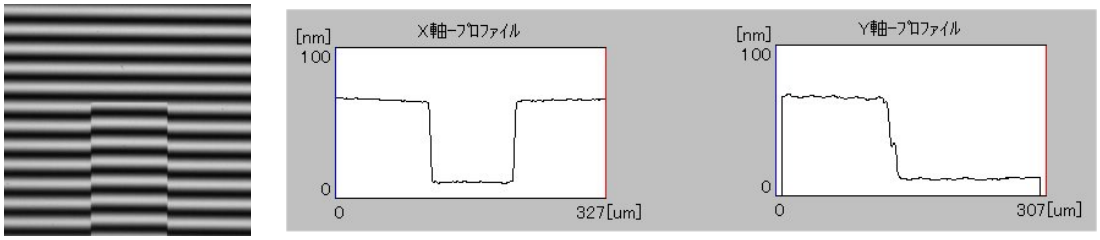

(a) Fringe image (b) Obtained surface profiles

Fig. 10-4 Horizontal fringe image and its measurement results

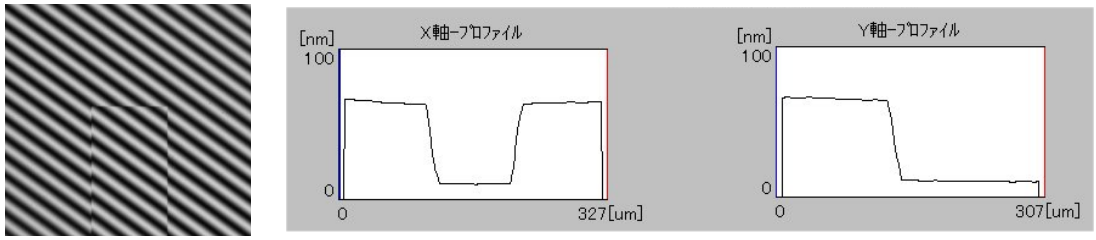

(a) Fringe image (b) Obtained surface profiles

Fig. 10-5 Slanted fringe image and its measurement results

10.2.3 In the case of curved or inclined surface samples

(1) Theoretical considerations

In this section, we consider what kind of difference occurs between vertical and horizontal fringe directions when there are locally inclined areas, as shown in Fig. 10-6(a). When a carrier fringe is introduced in the *x*-axis direction by tilting the reference surface at an inclination angle θ, a fringe pattern shown in Fig. 10-6(b) is formed. The following two conditions are necessary for the correct profile measurement from the interference fringes:

$$\theta - \varphi_1 > 0 \tag{10–1}$$

$$\theta + \varphi_2 < \phi_{\max} \tag{10–2}$$

where $\phi_{\max}$ is the angle at which the fringes becomes too dense and exceed the imaging resolution. It depends on the pixel resolution and wavelength of the imaging system. In particular, it should be noted that, when the value of $(\theta - \varphi_1)$ in Eq. (10-1) becomes small, the accuracy of the phase measurement decreases due to the increase of the fringe spacing, and when it becomes negative, it leads to incorrect results.

On the other hand, when a horizontal fringe is introduced, the fringes becomes parallel as shown in Fig. 10-7, and there is no such condition as in the case of vertical fringes. Therefore, horizontal fringes are suitable for measuring curved surfaces that are inclined in the horizontal (*x*-axis) direction[1)]. This conclusion is the same as for the step samples described in the previous section.

[1)] This fact seems to be self-evident in three-dimensional measurement by optical sectioning or stripe pattern projection methods.

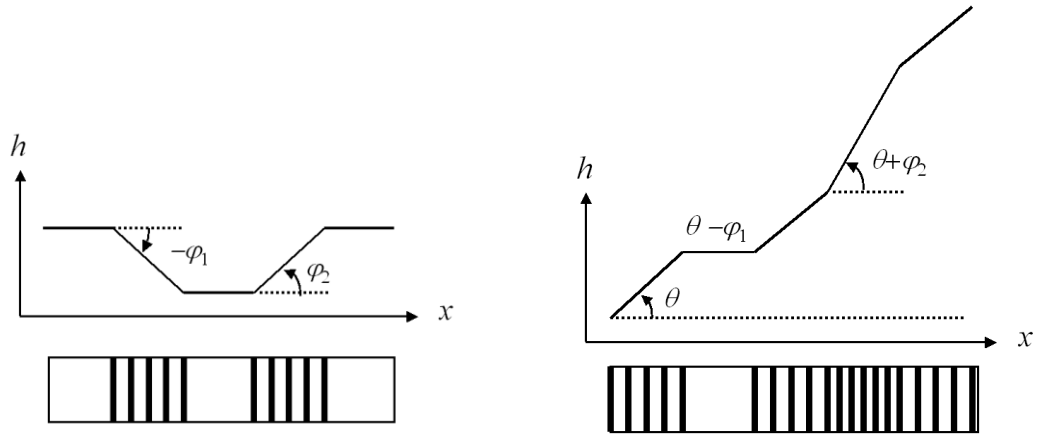

(a) Without spatial carrier (b) With spatial carrier

Fig. 10-6 Vertical fringe pattern of surface with slopes

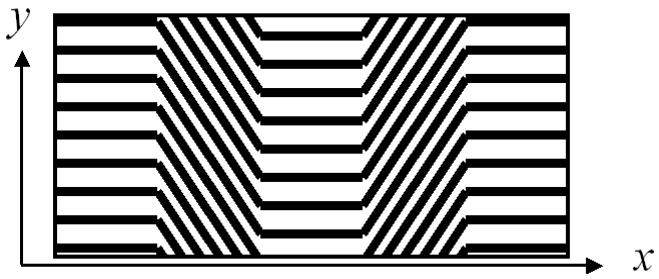

Fig. 10-7 Horizontal fringe pattern of surface with slopes

(2) Actual experiments

A metal surface with a convex cylindrical shape was measured by changing the direction of the fringes. The data area used was a long rectangle (5 × 25 pixels) in the direction orthogonal to the interference fringes. Images of vertical, horizontal and slanted fringes and the results of height measurements are shown in Fig. 10-8, 10-9 and 10-10. In the case of vertical fringes, the direction of carrier fringe introduction is downward to the left, but the slope is still negative in the region from the center to the right, so the measurement is not correct. On the other hand, with the horizontal fringes, the shape is measured correctly.

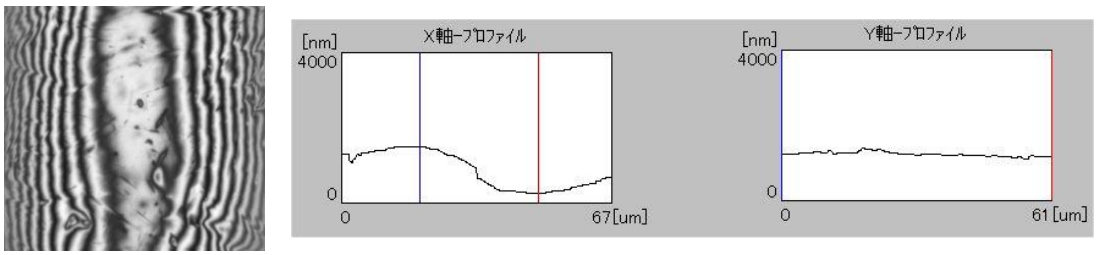

(a) Fringe image (b) Obtained surface profiles

Fig. 10-8 Vertical fringe image and its measurement results

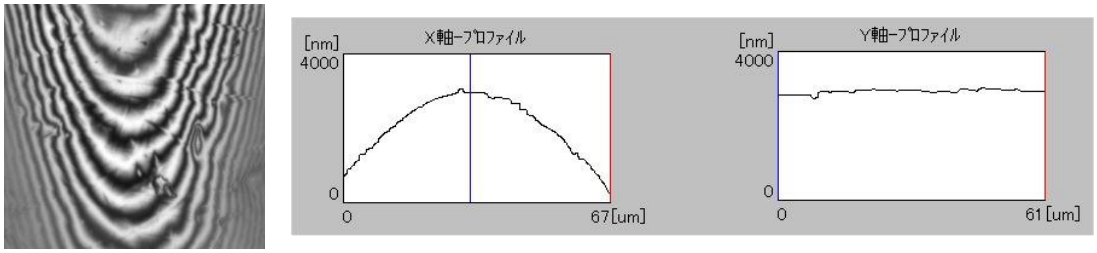

(a) Fringe image (b) Obtained surface profiles

Fig. 10-9 Horizontal fringe image and its measurement results

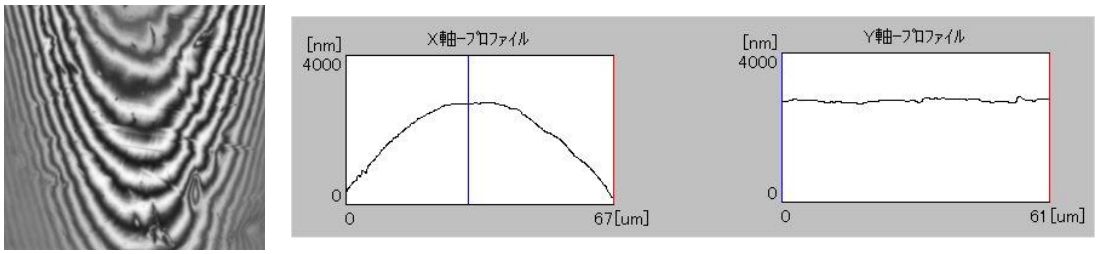

(a) Fringe image (b) Obtained surface profiles

Fig. 10-10 Slanted fringe image and its measurement results

10.2.4 Fringe direction selection for color filters

Considering the findings obtained so far, the color filter substrate was measured with different fringe directions. The phase at each point was determined by the LMF method, and the data area used was a long rectangle (5 × 25 pixels) in the direction orthogonal to the interference fringes. Fringe images and height measurement results (colored height images, *x*-axis profiles and *y*-axis profiles) for vertical, horizontal and slanted fringes are shown in Fig. 10-11, 10-12 and 10-13. The profile is a profile on the line passing through the center pixel of the image. The best lateral (*x*-axis) profile was obtained with the horizontal fringes. Therefore, horizontal fringes were adopted as the standard condition for this measurement system.

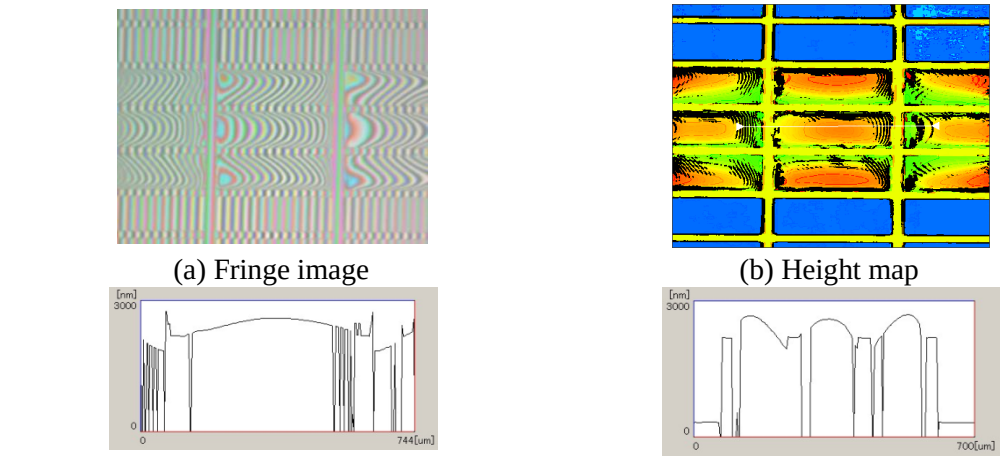

(a) Fringe image (b) Height map

(c) Horizontal profile (d) Vertical profile

Fig. 10-11 Vertical fringe image and its measurement results

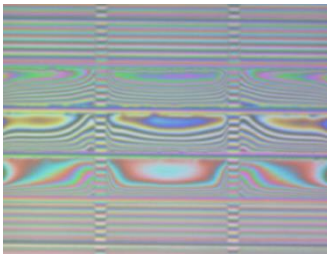

(a) Fringe image

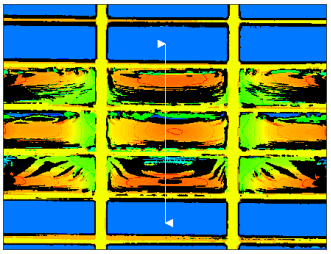

(b) Height map

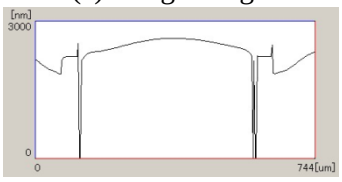

(c) Horizontal profile

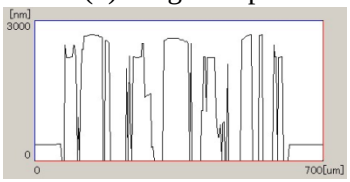

(d) Vertical profile

Fig. 10-12 Horizontal fringe image and its measurement results

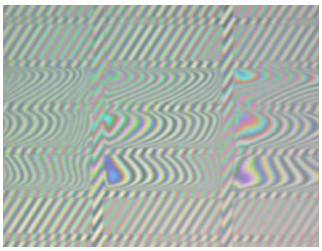

(a) Fringe image

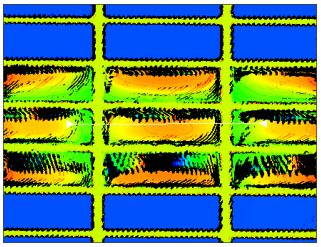

(b) Height map

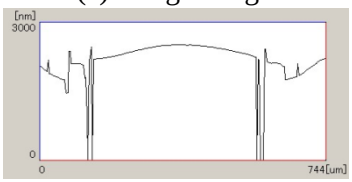

(c) Horizontal profile

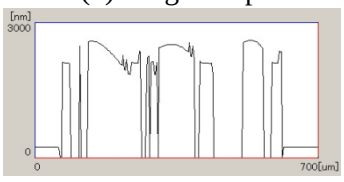

(d) Vertical profile

Fig. 10-13 Slanted fringe image and its measurement results

10.3 System configuration and automation techniques

10.3.1 Overall structure

An external view of the system is shown in Fig. 10-14. This is a commercially available 3-axis orthogonal robot (JR2503N made by Janome Sewing Machine Co. Ltd.) with a measurement optical system mounted. No special anti-vibration measures are taken. The target is an IJ color filter substrate with a maximum size of 510 × 510 mm. The standard objective lens magnification is 5x, and the field of view in this case is 1.25 × 0.95 mm. The camera has a high resolution (1344 × 1024 pixels), so the horizontal resolution (pixel size) is 0.92 μm. The computer used is a Windows PC with a 2GHz CPU, which enables fully automated measurement, including auto-focusing and image alignment.

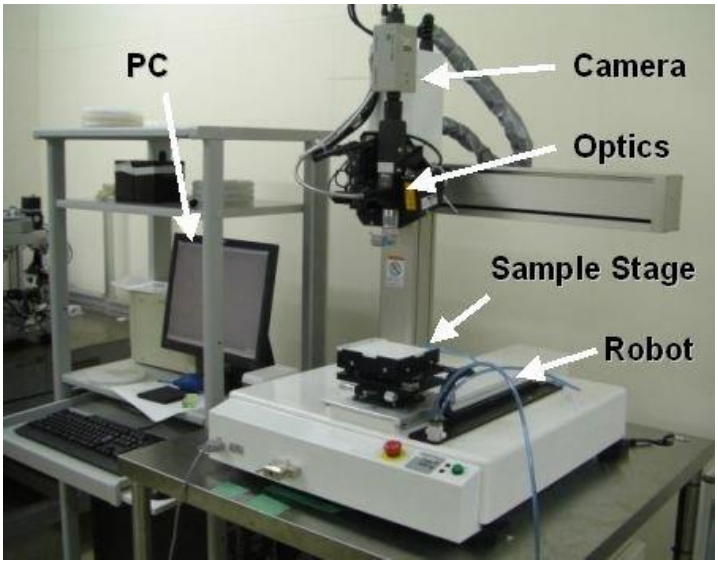

Fig. 10-14 Outlook of apparatus

10.3.2 Operation flow

The operation flow is shown below. Here, the stage movement is executed in parallel with the calculations of (3) to (5).

(1) Auto-focus
(2) Image Acquisition
(3) Alignment (position recognition)
(4) Height Calculation
(5) Film Thickness Calculation
(6) Move to the next stage >>> Return to (1).

10.3.3 Auto-focus

The distance between the optical system and the target surface varies due to the unevenness of the substrate and vertical movement of the stage. Maintaining this distance at a constant level is called "auto-focus". The auto-focus performance required in this system is determined by the following requirements: (1) the interference fringes must be observed over the entire image within the coherence length (approximately 20 μm); (2) the zero-order fringe must be in the image (± 6 μm in the case of 40 fringes).

In this system, the surface profile is measured on each image, and the absolute height, not the relative height, is obtained by considering the interference order and used for the autofocus. In practice, before capturing the next image, the Z-axis of the robot is controlled using the height measurement results of the previous image, because the vertical variation between images is within the acceptable range.

10.3.4 Alignment

For an automatic system such as our system, it is important to detect the positional error of each image by image processing technique and to correct the positional error by software. However, due to the presence of fringes in interference images, normal alignment techniques such as template matching cannot be used.

As an algorithm to remove fringes in interference fringe images, there is a proposal to use multiple images [Kitagawa et al. 2008c]. However, there is no algorithm for removing fringes

from a single image. The author tested methods such as (1) edge detection by a differential operator; (2) fringe frequency removal by the Fourier transform, but none of these methods yielded good results.

Therefore, we developed an alignment method of using a phase image instead of a fringe image. The phase is obtained from the captured image using the LMF method. The phase image is a density expression obtained by converting the phase values of $-\pi$ to π into 0 to 255, and is shaded according to the height as shown in Fig. 10-15. Therefore, as shown in Fig. 10-16, the empty cell region clearly appears as a dark rectangle or as a bright rectangle, and can be detected by conventional image processing alignment techniques (e.g., Blob analysis of binarized images).

As shown in Fig. 10-15, three phase images are obtained from a fringe image and they show different aspects, so that stable alignment is possible by selecting the most appropriate phase image for alignment.

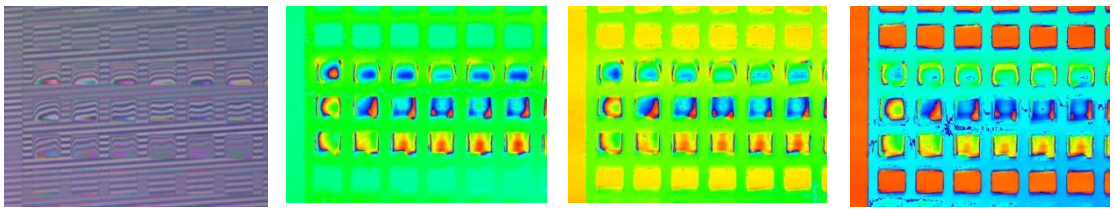

(a) Fringe image (b) Phase-B (c) Phase-G (d) Phase-R

Fig. 10-15 Fringe image and three phase images

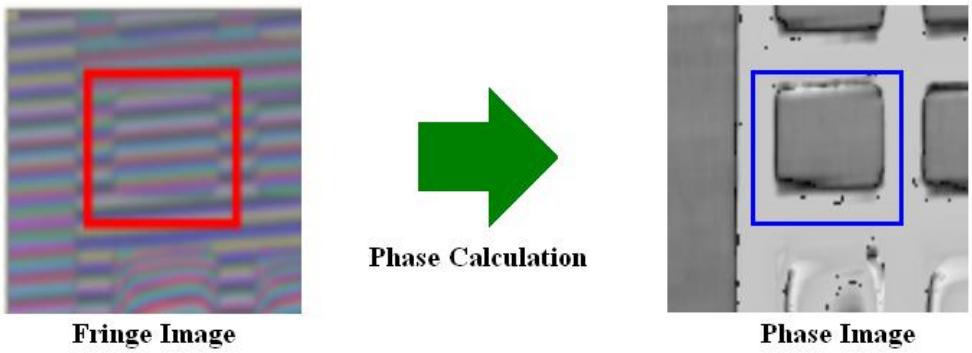

Fig. 10-16 Alignment by using phase image

10.4 Experimental results

10.4.1 Film thickness measurement

Examples of interference fringe images and measurement results are shown in Fig. 10-17 and Fig. 10-18. The results agree well with those of the conventional method (vertical scanning interferometry), except for the noise at the edges.

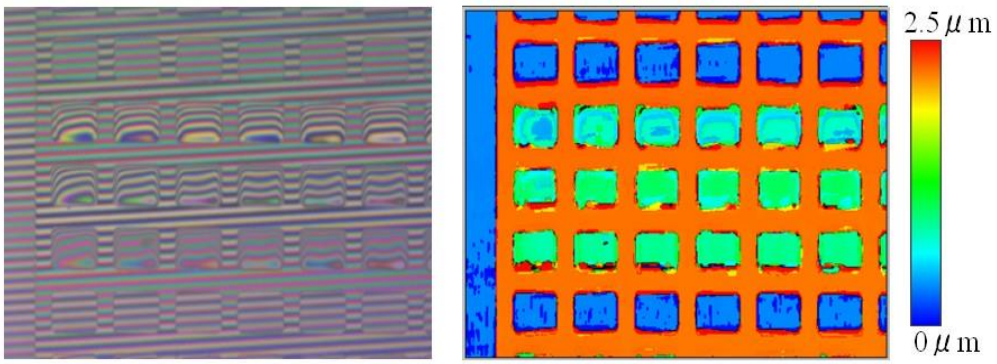

(a) Fringe image (b) Measured height

Fig. 10-17 Measurement of color filter

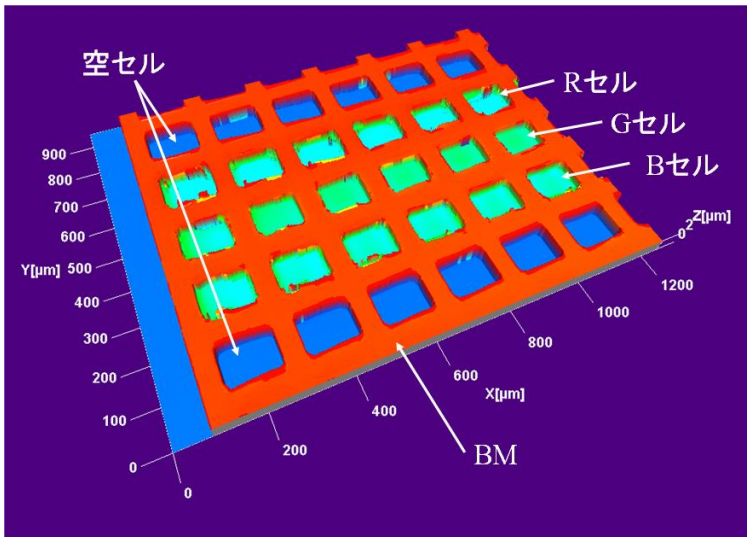

Fig. 10-18 Measured height of color filter (3D view)

10.4.2 Measurement accuracy

Table 10-1 shows the measured film thicknesses during repeated measurements. The film thickness was determined as the average value of the central rectangular region (size: 70 × 40 pixels) of each cell. The values in this table are the average of the six cells of each color. The reproducibility (σ) is very good at about 1 nm.

Table 10-1 Measurement repeatability of thickness (nm)

Color	R	G	B
Average	515	700	773
Standard deviation (σ)	1.0	0.9	1.6

10.4.3 Measurement speed

Initially, the measurement speed during automatic measurement was about 8 s per field of view, but it was shortened to 1.5 s by subsequent improvements. The details are described in the next section.

10.5 Improvements of the measurement system

10.5.1 Background and objectives of the study

The automatic film thickness measurement system for color filter substrates described in the previous sections has achieved the intended goal and has been put into practice. The result of the time analysis for each process is shown in Fig. 10-19. From this result, it can be seen that it takes time in the order of image acquisition, phase calculation, and height calculation. Therefore, we investigated the speed-up of each of these three processes.

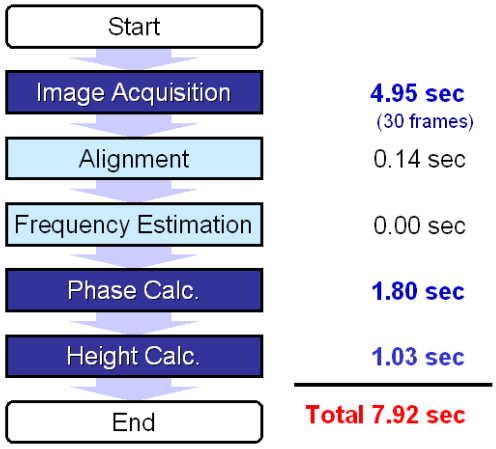

Fig. 10-19 Results of execution time analysis

10.5.2 Reduction of image acquisition time by new lighting system

(1) Problems in image acquisition

Although single-shot interferometry is a vibration-resistant measurement method, automatic film thickness measurement systems were still vulnerable to vibration for the following reasons.

(a) Insufficient light: A narrow bandpass filter with a half-width of 10 nm was used to increase the coherence length of the illumination light. Because of this, the light intensity was insufficient and the exposure time of the camera could not be reduced to 1/500 s, which is the target exposure time, and had to be 1/200 s.
(b) Vibration resistance: A commercially available three-axis robot was used for the main body of the machine, and no special measures was taken for vibration isolation. This was partly because we did not consciously select anti-vibration equipment for the concept of the single-shot interference measurement method.

In the captured image, there were many subject blurs due to vibration as shown in Fig. 10-20, and measurement errors occurred frequently. As a countermeasure, 30 images were continuously acquired per measurement, and the image with the least subject blur was selected from these images. For this reason, the image acquisition time including image selection was as long as about 5 s.

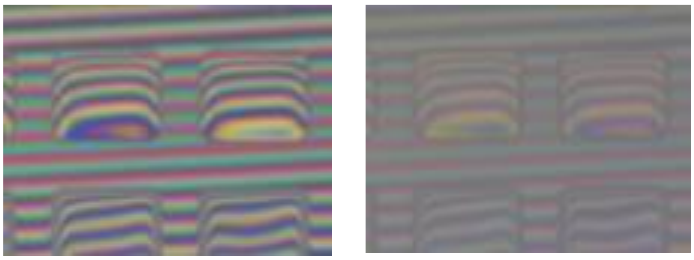

(a) Without blur (b) With blur

Fig. 10-20 Captured images without and with motion blur

(2) New lighting system

In order to suppress the blurring of the subject, it is effective to increase the shutter speed, but it is not easy to increase the sensitivity of the camera or the light intensity of the light source. Therefore, we focused on the configuration of the optical system and studied the improvement of the illumination path.

The conventional lighting system consists of three halogen lamp light sources, each of which has a narrow-bandwidth transmission filter attached to it, and they are mixed and irradiated by a three-branch optical fiber light guide, as shown in Fig. 9-21. Therefore, the light path of each wavelength is limited to 1/3 of the total light path of the light guide.

To improve this bottleneck in the optical path, we have developed and introduced optical filters called Multi-Bandpass Filters (MBPFs). This filter differs from an ordinary bandpass filter in that it can transmit light in multiple bands as shown in Fig. 10-21.

The introduction of this filter made it possible to obtain a mixture of three wavelengths of light from a single light source, as shown in Fig. 10-22. Since the transmittance could be designed to be higher than that of the conventional filter, the amount of illumination light was finally five times that of the conventional filter, and the shutter speed was improved from 1/200 s to 1/1000 s. As a result, it is less susceptible to vibration, and the number of images taken per measurement was reduced to three, and the imaging time was reduced from 4.95 s to 1.12 s. The number of light sources has been reduced to one-third, and the manufacturing and running costs of the system have been significantly reduced. The effects of introducing MBPF are shown in Table 10-2.

The MBPF is usually used for Raman spectroscopy, and there are no examples of its use in the illumination of multi-wavelength interferometry.

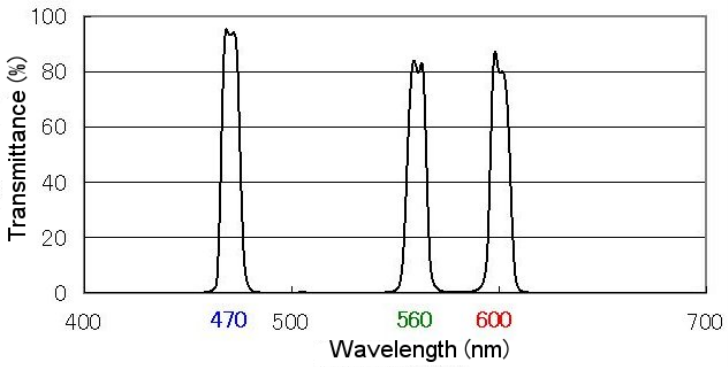

Fig. 10-21 Spectral transmittance of multi-bandpass filter

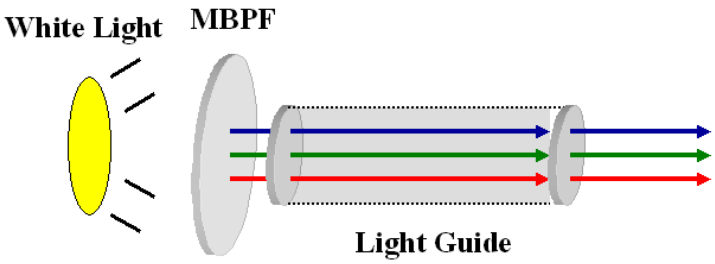

Fig. 10-22 New three-wavelength illumination system

Table 10-2 Effect of MBPF

Items	Conventional method	MBPF method
Shutter speed (camera)	1/200 s	1/1000 s
Number of images required	30	3
Required time	4.95 s	1.12 s
Number of filters	3	1
Number of illuminators	3	1

10.5.3 Speed-up by parallel processing

The phase calculation by the LMF method is a neighborhood operation of each pixel, and the height calculation is a pixel-independent calculation. Therefore, we introduced the following two methods.

(1) Introduction of multi-core processing

In recent years, computer CPUs have shifted from increasing frequency to increasing the number of cores as an approach to improve processing power. Therefore, we divided the image into several images as shown in Fig. 10-23 to optimize the parallel processing and the software for the multi-core CPUs. As a result, the phase and height calculations were accelerated by a factor of 3.1 and 6.4, respectively.

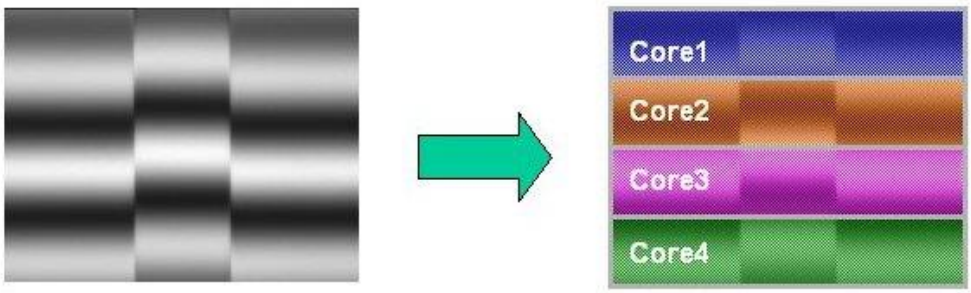

Fig. 10-23 Speed-up by multi-core technology

(2) Introduction of GPGPU parallel processing

The GPGPU (General Purpose Computing on GPU) technology, which has been attracting a lot of attention in recent years, was introduced to increase the speed of the system. As shown in Fig. 10-24, this technique enables us to accelerate the computation by performing parallel computing on a large number of cores on the GPUs (Graphics Processing Unit).

The advantages of GPGPUs are as follows.

- Optimized for parallel computing using the same algorithm.
- A complete set of development tools is available, and the hurdles to introducing the system are relatively low.
- Compared to CPUs, there is more room for growth in processing capacity, and further improvements in speed can be expected in the future.
- The installation cost is low (about 40,000 yen for general-purpose products and about 200,000 yen for business use).

On the other hand, the disadvantages are the following.

- It is not good at branching (it can be done, but the operation time is much slower than the CPU).
- It takes time to transfer data to the GPU (depending on the amount of computation, the CPU may be faster than the GPU).

Height calculation cannot be expected to be effective because search (branch processing) is the main processing, but phase calculation can be expected to be effective because most of it is matrix operation processing that GPGPU is good at. Therefore, we introduced a GPU (NVIDIA QuadroFX4600, 96 cores) for the phase calculation. As a result, the phase computation time was 10.6 times faster than that of the single CPU processing, and 3.1 times faster than that of the multi-core processing, and the processing time per field of view was significantly reduced to 0.17s.

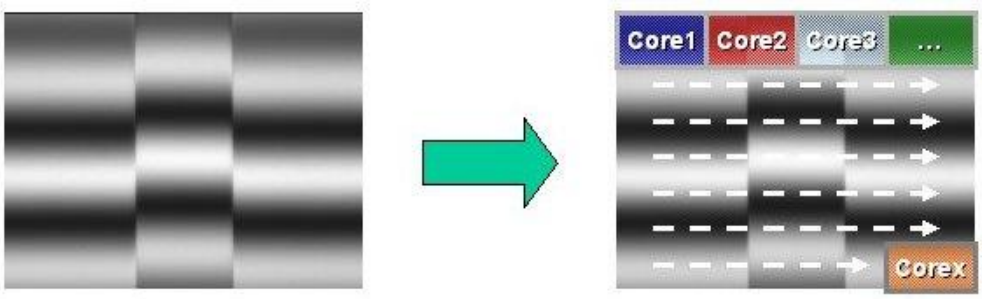

Fig. 10-24 Speed-up by GPGPU technology

10.5.4 Speed-up of height calculation by LUT method

Height calculation by the coincidence method is a process of searching for the most probable height value from the phases of three wavelengths, but there are a finite number of meaningful phase combinations. Therefore, if the heights for the combinations of phases are stored in advance as a dictionary (lookup table, or LUT), the search process can be eliminated during the measurement, as shown in Fig. 10-25.

The size of the phase combination table depends on the phase step. Based on the experimental results of the coincidence method, assuming the required height step of three nm, the phase step is approximately $2\pi/100$, and the table size becomes $100^3=10^6$.

The parameters of this table are three wavelengths and the order search range, and when

they are changed, the table is newly created. At run time, we only need to read the orders from the phases of the three wavelengths.

We consider the effect of introducing a lookup table in the height calculation in the three-wavelength coincidence method. Comparing the number of height calculations for each pixel, when the order range is N, it is $3N$ times in the conventional method, but one time in the LUT method. When the height range is 4 μm, the order range N is 14, so the operation times ratio is 42:1.

As a result of this improvement, the processing time for the height calculation was reduced to 0.06 s, which is 17.2 times faster than that of the single-core system and 6.4 times faster than that of the multi-core system.

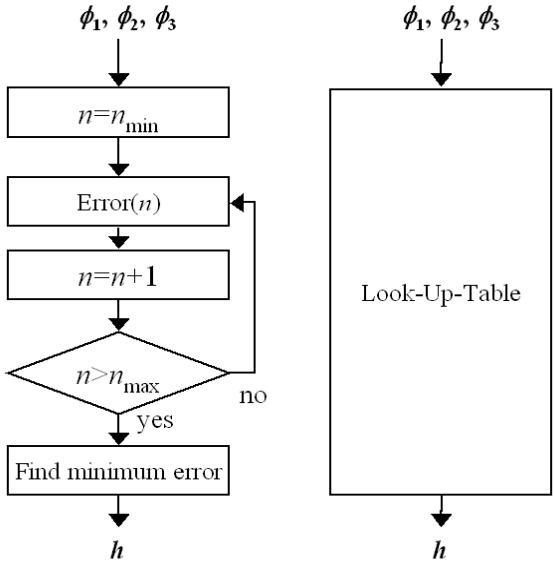

(a) Before (b) After

Fig. 10-25 Speed-up by Look-Up-Table method

10.5.5 Results of improvements

The speed of the automatic color filter film thickness measurement system was increased. Image acquisition and selection times have been greatly improved by the development of a new illumination system using multi-band filters, phase calculation by adopting multi-core and GPU, and height calculation by adopting the Look-Up-Table method, respectively. Details of the measurement time before and after the speed-up are shown in Table 10-3. As a result, the time required per image was reduced from 7.9 s to 1.5 s.

Table 10-3 Improvement of measurement time

	Before improvement (s)	After improvement (s)
Image capture	4.95	1.12
Alignment	0.14	0.14
Frequency estimation	0.00	0.00
Phase calculation	1.80	0.17
Height calculation	1.03	0.06
Total	7.92	1.49

10.6 Summary

An automatic film thickness measurement system for ink-jet color filters has been developed using the three-wavelength single-shot method. First, the effect of the direction of the introduced fringes was considered, and it was demonstrated that horizontal fringes were better than vertical fringes in the case of this measurement target.

Next, we developed the auto-focus and alignment techniques necessary for automation. Both of them were realized by fringe image processing without any new hardware.

From the test results with actual samples, it was confirmed that the measurement repeatability on the nanometer order was achieved without any special vibration isolation mechanism.

In order to further improve the vibration resistance and speed of the system, we have developed a high-brightness three-wavelength illumination method using a multi-bandpass filter (MBPF). We have also reduced the computation time by more than one digit by adopting the GPU and developing a Look-Up-Table height calculation algorithm. As a result, an automatic film thickness measurement system with a high measurement speed of 1.5 s per image (1.5 μs per pixel) has been developed.

This is an English translation of the article:
Katsuichi Kitagawa, "Chapter 10: Automatic film thickness measurement system for ink-jet type color filters",
in "Study on industrial surface profile measurement method based on optical interferometry", pp. 120-134, Doctoral Dissertation, University of Tokyo (2011)
(original in Japanese; translated by the author in Oct. 2020)